

Electronic supplementary information

Direct Evidence for an Interdiffused Intermediate Layer in Bi-Magnetic Core-Shell Nanoparticles

Amélie Juhin^{*a}, Alberto López-Ortega^{*b,c}, Marcin Sikora^d, Claire Carvallo^a, Marta Estrader^{b,e}, Sònia Estradé^{f,g}, Francesca Peiró^f, Maria Dolors Baró^h, Philippe Saintavit^a, Pieter Glatzelⁱ and Josep Nogués^{b,h,j}

^aInstitut de Minéralogie, de Physique des Matériaux et de Cosmochimie (IMPMC), Sorbonne Universités, UMR CNRS 7590, UPMC Univ Paris 06, Muséum National d’Histoire Naturelle, IRD UMR 206, 4 Place Jussieu, F-75005 Paris, France.

^bICN2 – Institut Català de Nanociència i Nanotecnologia, Campus UAB, E-08193 Bellaterra (Barcelona), Spain.

^cINSTM and Dipartimento di Chimica “U. Schiff”, Università degli Studi di Firenze, Via della Lastruccia 3, Sesto Fiorentino, I-50019 Firenze, Italy.

^dAGH University of Science and Technology, Faculty of Physics and Applied Computer Science & Academic Centre for Materials and Nanotechnology, Al. Mickiewicza 30, PL-30-059 Kraków, Poland. ^eDepartament de Química Inorgànica, Universitat de Barcelona, Diagonal 647, E-08028, Barcelona, Spain.

^fLENS-MIND-IN2UB, Departament d’Electrònica, Universitat de Barcelona, Martí i Franquès 1, E-0828 Barcelona, Spain.

^gTEM-MAT, CCiT, Universitat de Barcelona, Barcelona, Spain.

^hDepartament de Física, Universitat Autònoma de Barcelona, E-08193 Bellaterra (Barcelona), Spain.

ⁱEuropean Synchrotron Radiation Facility, CS40220, F-38043 Grenoble Cedex 9, France.

^jInstitució Catalana de Recerca i Estudis Avançats (ICREA), Barcelona, Spain.

Corresponding authors: lopezortega.alberto@gmail.com. *E-mails: Amelie.Juhin@impmc.upmc.fr;

1. Morphological-structural characterization

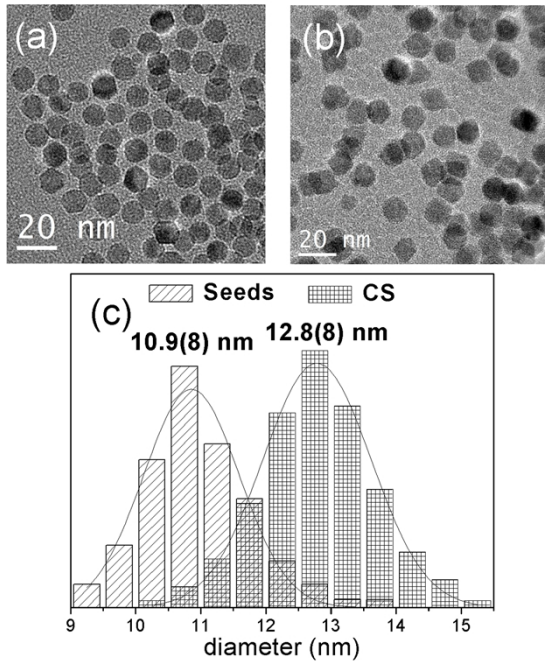


Figure S1. TEM images of (a) the seeds and (b) the CS nanoparticles. (c) Particle size histograms of the seeds and the CS nanoparticles, fitted to a Gaussian distribution.

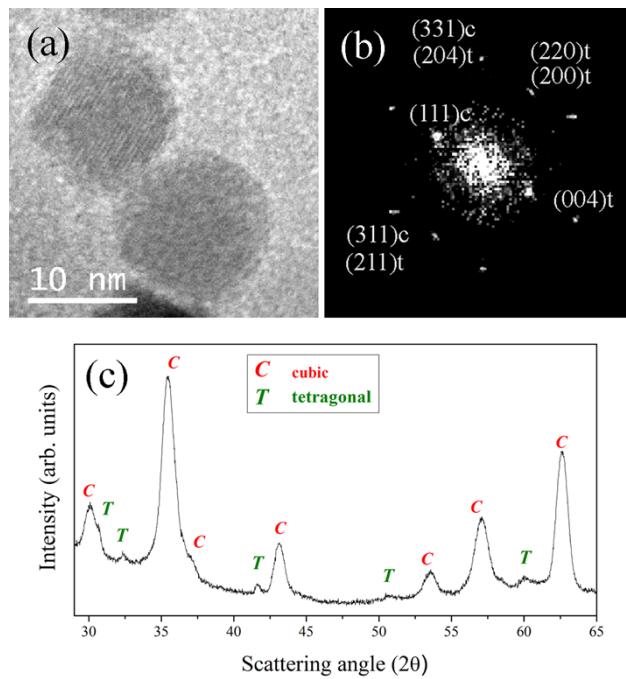


Figure S2. (a) HR-TEM image of CS nanoparticles and (b) its corresponding FFT with the spots indexed. Spots are marked by *c* or *t* for cubic and tetragonal spinels, respectively. (c) Powder X-ray diffraction of the CS nanoparticle. The peaks are indexed by *C* or *T* for cubic and tetragonal spinel structures, respectively.

2. Magnetic characterization

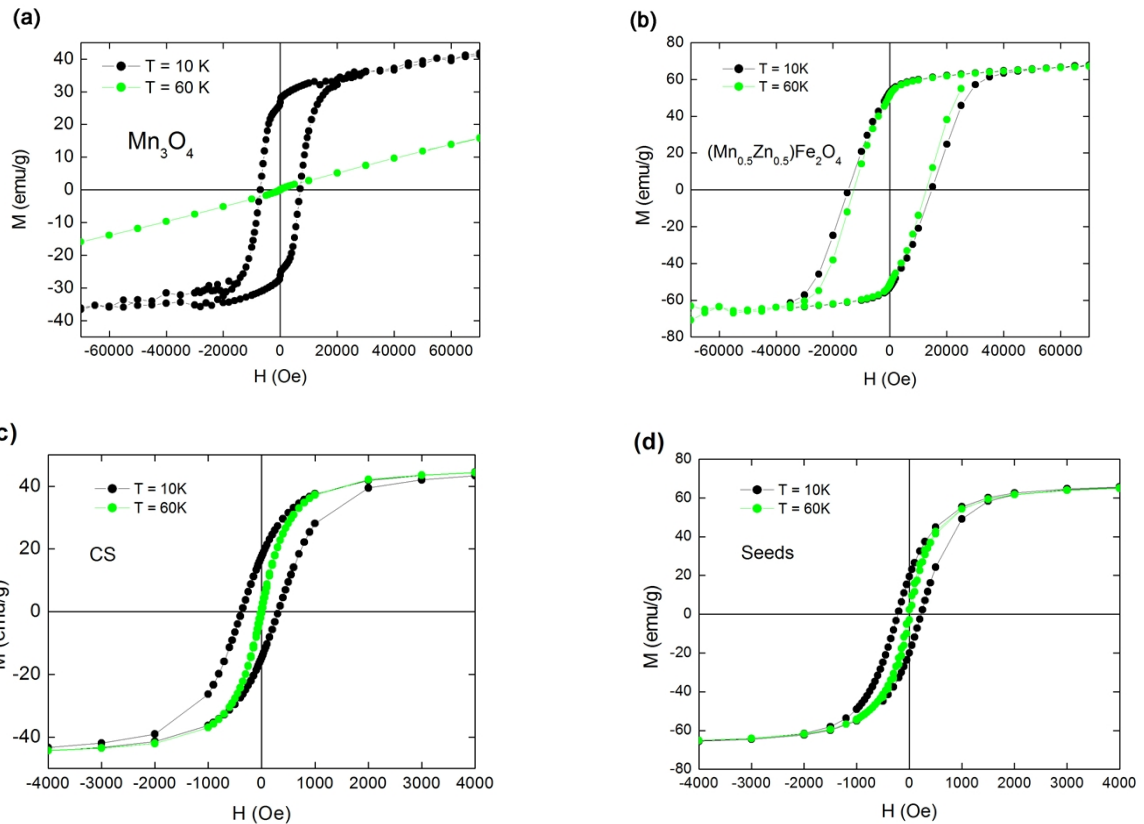


Figure S3. Magnetization curves measured with SQUID magnetometer on the Mn_3O_4 reference sample (a), the $\text{Mn}_{0.5}\text{Zn}_{0.5}\text{Fe}_2\text{O}_4$ nanoparticles (b), and the CS (c) and the seed samples (d).

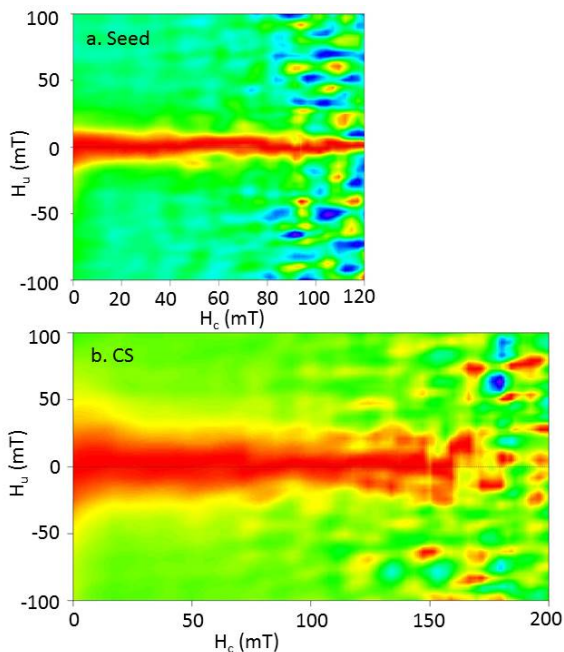


Figure S4. Normalized FORC diagrams at $T = 20\text{ K}$ obtained by dividing the FORC distribution in each vertical column by the maximum value in that column. (a) Seed sample, (b) CS nanoparticles.

3. RIXS-MCD spectrum of magnetite.

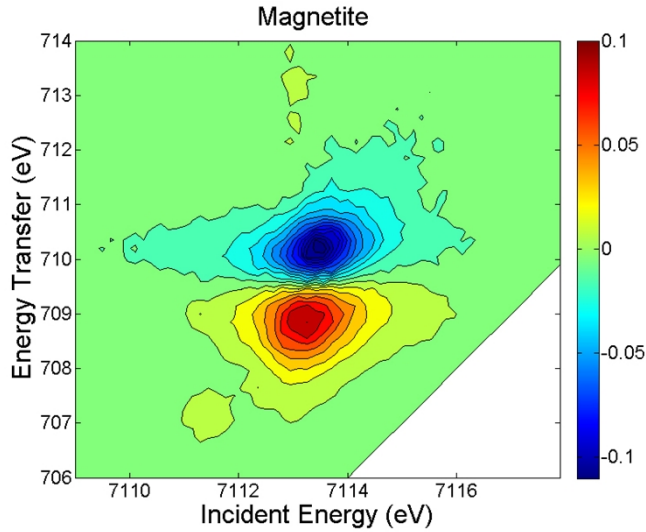


Figure S5. Room temperature RIXS-MCD spectrum measured for magnetite at the Fe *K* pre-edge. The spectrum is replotted after Ref. S1 and normalized to the pre-edge maximum.

4. Growth of the Mn_3O_4 shell

As suggested by Salazar-Alvarez et al,^{S2} the growth of manganese oxide over iron oxide nanoparticles takes place by an intermediate step driven by the initial deposition of MnO followed by its surface passivation to form Mn_3O_4 . Note that because of Mn^{2+} vacancies in (111) MnO planes, the O^{2-} arrangement presents an atomic coordination similar to the one of Fe^{3+} atoms in the (111) planes of maghemite. This results in an effective cell parameter for the MnO (111) planes of 0.297 nm, whereas the equivalent doubled cell parameter is 0.596 nm for (111) planes of maghemite. Consequently the lattice mismatch is smaller than 1%. In addition, manganese surface passivation is accompanied by ion diffusion from the core to the shell and vice versa, forming a graded interface between $\gamma\text{-Fe}_2\text{O}_3$ and Mn_3O_4 stabilizing the structure mismatch between both layers.

5. Quantitative modeling of the CS internal structure.

We consider that all particles are identical in size and shape. Their structure is described by an onion like profile (figure S6), where:

- the inner shell (radius b and volume $V_{inner} = 4/3 \pi(b^3 - a^3)$) is built from manganese iron oxide $(\text{MnFe})_3\text{O}_4$ with statistical cationic repartition $[\text{Mn}_{0.5}\text{Fe}_{0.5}]_{\text{tetra}} [\text{Mn}_{1.0}\text{Fe}_{1.0}]_{\text{octa}} \text{O}_4$.
- the outer shell (radius c and volume $V_{outer} = 4/3 \pi(c^3 - b^3)$) is built from manganese oxide $[\text{Mn}_{1.0}]_{\text{tetra}} [\text{Mn}_{2.0}]_{\text{octa}} \text{O}_4$.

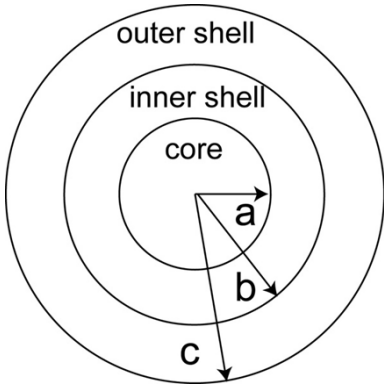


Figure S6. Onion like structure considered for the quantitative analysis of RIXS-MCD data.

At the Mn edge, only the inner shell contributes to the MCD, but both the inner and outer shells contribute to the XAS. Table S1 summarizes the contribution of every shell in the model CS particle to the intensity of the absorption, I_{XAS} , and to the intensity of the MCD, I_{MCD} , at the Mn edge. $I_{\text{XAS}}^{\text{O}}$ and $I_{\text{XAS}}^{\text{T}}$ are the contributions to the XAS of a Mn ion in octahedral site and in tetrahedral site, respectively. $I_{\text{MCD}}^{\text{O}}$ and $I_{\text{MCD}}^{\text{T}}$ are the contributions to the MCD of a Mn ion in octahedral site and in tetrahedral site respectively.

Table S1. Contribution of every shell in the CS particle to the intensity of absorption I_{XAS} and of magnetic circular dichroism I_{MCD} at the Mn edge.

Mn edge	I_{MCD}	I_{XAS}
Outer shell in CS:		
$[\text{Mn}_{1.0}]\text{tetra}[\text{Mn}_{2.0}]\text{octa}\text{O}_4$	0	$V_{\text{outer}} (I_{XAS}^T + 2I_{XAS}^O)$
Inner shell in CS:		
$[\text{Mn}_{0.5}\text{Fe}_{0.5}]\text{tetra}$	$V_{\text{inner}} * (0.5 * I_{MCD}^T + I_{MCD}^O)$	$V_{\text{inner}} * (0.5 * I_{XAS}^T + I_{XAS}^O)$
$[\text{Mn}_{1.0}\text{Fe}_{1.0}]\text{octa}\text{O}_4$		
Core in CS:		
$[\text{Fe}_{1.0}]\text{tetra}[\text{Fe}_{5/3}]\text{octa}\text{O}_4$	0	0
Total in CS	$V_{\text{inner}} * (0.5 * I_{MCD}^T + I_{MCD}^O)$	$V_{\text{outer}} (I_{XAS}^T + 2I_{XAS}^O) + V_{\text{inner}} * (0.5 * I_{XAS}^T + I_{XAS}^O)$

The normalized MCD for the whole CS particle is:

$$I_{MCD}^{CS}/I_{XAS}^{CS} = \frac{(0.5I_{MCD}^T + I_{MCD}^O)V_{\text{inner}}}{(I_{XAS}^T + 2I_{XAS}^O)V_{\text{outer}} + (0.5I_{XAS}^T + I_{XAS}^O)V_{\text{inner}}} \quad (\text{Equation S1})$$

We now assume that: $I_{XAS}^O = |\alpha| I_{XAS}^T$ and $I_{MCD}^O = \alpha I_{MCD}^T$.

This is based on the following arguments: (i) site distribution in the above mentioned spinel oxides is too complex to precisely account for (both Fe and Mn occur at tetrahedral and octahedral sites) since individual contributions are difficult to disentangle, (ii) In the K pre-edge region the contribution of tetrahedral sites dominates the XAS over that of octahedral sites, since the lack of inversion centre in T_d symmetry allows electric dipole transitions which are more intense than electric quadrupole contributions. Ligand field multiplet calculations have enabled to quantify their respective intensities in the case of Fe^{2+} and Fe^{3+} for several oxides, showing that the K pre-edge for a tetrahedral site is ~4-5 times higher than for an octahedral site.^{S3} We further assume that tetrahedral sites contribute to the MCD stronger than the octahedral sites in the same proportion, i.e., 5 times larger than the octahedral sites but with the opposite sign due to the antiferromagnetic coupling. This yields $\alpha = -0.2$. Note that this value was determined from the relative intensities of HERFD-MCD measured for maghemite (11 % peak-to-peak, Figure 3b) and magnetite (16 % peak-to-peak) reference samples,^{S1} taking into account their respective cationic repartition.

Equation (S1) now yields:

$$I_{MCD}^{CS}/I_{XAS}^{CS} = (I_{MCD}^T/I_{XAS}^T) * \frac{V_{inner} * (0.5 + \alpha)}{(0.5 + |\alpha|) * V_{inner} + (1 + 2|\alpha|) * V_{outer}} \quad (\text{Equation S2})$$

$I_{MCD}^{CS}/I_{XAS}^{CS}$ is the value determined from the HERFD-MCD spectrum of the CS particles. We use the peak-to-peak value $I_{PP}(CS)$.

(I_{MCD}^T/I_{XAS}^T) is determined from the HERFD-MCD measured on a reference sample with 100% tetrahedral Mn, *i.e.*, $\text{Mn}_{0.5}\text{Zn}_{0.5}\text{Fe}_2\text{O}_4$. We use the peak-to-peak value $I_{PP}(\text{Mn}_{0.5}\text{Zn}_{0.5}\text{Fe}_2\text{O}_4)$.

$$\text{We obtain: } I_{PP}(CS) = \frac{V_{inner} * (0.5 + \alpha)}{(0.5 + |\alpha|) * V_{inner} + (1 + 2|\alpha|) * V_{outer}} I_{PP}(\text{Mn}_{0.5}\text{Zn}_{0.5}\text{Fe}_2\text{O}_4) \quad (\text{Equation S3}).$$

At the Fe edge, both the inner shell and the core contribute to the MCD and to the XAS. Table S2 summarizes the contribution of every shell in the model CS particle to the absorption, I'_{XAS} , and to the intensity of the MCD, I'_{MCD} , at the Fe edge. I'_{XAS}^O and I'_{XAS}^T are the contributions to the XAS of a Fe ion in octahedral site and in tetrahedral site, respectively. I'_{MCD}^O and I'_{MCD}^T are the contributions to the MCD of a Fe ion in octahedral site and in tetrahedral site respectively.

Table S2. Contribution of every shell in the CS particle to the intensity of absorption I_{XAS} and of magnetic circular dichroism I_{MCD} at the Fe edge.

Fe edge	I_{MCD}	I_{XAS}
Outer shell in CS:		
$[\text{Mn}_{1.0}]_{\text{tetra}}[\text{Mn}_{2.0}]_{\text{octa}}\text{O}_4$	0	0
Inner shell in CS:		
$[\text{Mn}_{0.5}\text{Fe}_{0.5}]_{\text{tetra}}[\text{Mn}_{1.0}\text{Fe}_{1.0}]_{\text{octa}}\text{O}_4$	$V_{inner} * (0.5 * I'_{MCD}^T + * I'_{MCD}^O)$	$V_{inner} * 0.5 * I'_{XAS}^T + V_{inner} * I'_{XAS}^O$
Core in CS:		
$[\text{Fe}_{1.0}]_{\text{tetra}}[\text{Fe}_{5/3}]_{\text{octa}}\text{O}_4$	$V_{core}(I'_{MCD}^T + 5/3 I'_{MCD}^O)$	$V_{core}(I'_{XAS}^T + 5/3 I'_{XAS}^O)$
Total in CS		
	$V_{inner} * (0.5 * I'_{MCD}^T + I'_{MCD}^O)$ + $V_{core}(I'_{MCD}^T + 5/3 I'_{MCD}^O)$	$V_{inner} * 0.5 * I'_{XAS}^T + V_{inner} * I'_{XAS}^O + V_{core}(I'_{XAS}^T + 5/3 I'_{XAS}^O)$

The normalized MCD for the whole CS particle is:

$$I'_{MCD}^{CS}/I'_{XAS}^{CS} = \frac{(I'_{MCD}^O + 0.5I'_{MCD}^T)V_{inner} + (I'_{MCD}^T + \frac{5}{3}I'_{MCD}^O)V_{core}}{(I'_{XAS}^O + 0.5I'_{XAS}^T)V_{inner} + (I'_{XAS}^T + \frac{5}{3}I'_{XAS}^O)V_{core}} \quad (\text{Equation S4})$$

We now assume again that: $I'_{XAS}^T = |\alpha| I'_{XAS}^O$ and $I'_{MCD}^T = \alpha I'_{MCD}^O$.

Equation (S4) yields:

$$I'_{MCD}^{CS}/I'_{XAS}^{CS} = (I'_{MCD}^T/I'_{XAS}^T) \frac{(0.5 + \alpha)*V_{inner} + (1 + 5\alpha/3)*V_{core}}{(0.5 + |\alpha|)*V_{inner} + (1 + 5|\alpha|/3)*V_{core}} \quad (\text{Equation S5})$$

$I'_{MCD}^{CS}/I'_{XAS}^{CS}$ is the value determined from the HERFD-MCD spectrum at the Fe edge of the CS particles. We use the peak-to-peak value $I'_{PP}(CS)$.

(I'_{MCD}^T/I'_{XAS}^T) is determined from the HERFD-MCD measured on the reference sample $\text{Fe}_{8/3}\text{O}_4$.

For $\text{Fe}_{8/3}\text{O}_4$, we use the peak-to-peak value:

$$I'_{PP}(\text{Fe}_{8/3}\text{O}_4) = (I'_{MCD}^T/I'_{XAS}^T) * \frac{1 + 5|\alpha|/3}{1 + 5\alpha/3}$$

Equation (S5) thus yields

$$I'_{PP}(CS) = \frac{(0.5 + \alpha)*V_{inner} + (1 + 5\alpha/3)*V_{core}}{(0.5 + |\alpha|)*V_{inner} + (1 + 5|\alpha|/3)*V_{core}} * \frac{1 + 5|\alpha|/3}{1 + 5\alpha/3} I'_{PP}(\text{Fe}_{8/3}\text{O}_4) \quad (\text{Equation S6}).$$

Supplementary references

- S¹. M. Sikora, A. Juhin, T.C. Weng, P. Sainctavit, C. Detlefs, F. de Groot, P. Glatzel, *Phys. Rev. Lett.* 2010, **105**, 037202.
- S². G. Salazar-Alvarez, H. Lidbaum, A. López-Ortega, M. Estrader, K. Leifer, J. Sort, S. Suriñach, M.D. Baró, J. Nogués, *J. Am. Chem. Soc.*, 2011, **133**, 16738-16741.
- S³. M.A. Arrio, S. Rossano, Ch. Brouder, L. Galoisy, G. Calas, *Europhys. Lett.* 2000, **51**, 454-460.